

Collective dynamics of periodic nonlinear oscillators under simultaneous parametric and external excitations

Diala Bitar · Najib Kacem · Nouredine Bouhaddi ·
Manuel Collet

Received: 14 November 2014 / Accepted: 1 June 2015

Abstract The collective dynamics of a periodic structure of coupled Duffing-Van Der Pol oscillators is investigated under simultaneous external and parametric excitations. An analytical computational model based on a perturbation technique, combined with standing wave decomposition and the asymptotic numerical method is developed for a finite number of coupled oscillators. The frequency responses and the basins of attraction are analyzed for the case of small arrays, demonstrating the importance of the multi-mode solutions and the robustness of their attractors. This model can be exploited to design periodic structure-based smart systems with high performance, by taking advantage of the multi-modes induced by the collective dynamics.

Keywords Collective dynamics, Nonlinear oscillators, Periodic structures, Asymptotic Numerical Method and Basins of attraction.

1 Introduction

Periodic structures consist of an arrangement of coupled identical substructures, geometrically repeated, defined by a unit cell at periodic intervals. They can exist naturally with

D. Bitar (✉) · N. Kacem · N. Bouhaddi
FEMTO-ST Institute, UMR 6174, Applied Mechanics Department,
University of Franche-Comté, (UBFC), 24 Chemin de l'Épitaphe,
F 25000, Besançon, France

D. Bitar
E-mail: diala.bitar@femto-st.fr

N. Kacem
E-mail: najib.kacem@femto-st.fr

N. Bouhaddi
E-mail: noureddine.bouhaddi@femto-st.fr

M. Collet
LTDS, UMR 5513, Ecole Centrale de Lyon,
36 avenue Guy de Collongue, F 69134, Ecully, France.
E-mail: manuel.collet@ec-lyon.fr

length scales as atomic lattices of pure crystals, as in many fields of engineering like turbines, long span bridges, multi-layered composites, stiffened plates, shells and so on.

Several researches on wave propagation in periodic structures were based on linear structural models. For instance, Brillouin [1] pointed his classic work on wave motion in simple periodic systems. Mead [2] presented a general theory of wave-propagation which is not restricted to flexural motion. In addition, Langley *et al.* [3] studied the response of a two-dimensional linear periodic structure subject to point harmonic forcing using a mass-spring model and presented theoretical and experimental studies to the response of a beam grillage [4]. Jensen [5], investigated the phononic band gaps and vibrations in one- and two-dimensional mass-spring structures. Moreover, Collet *et al.* [6] developed new multifunctional structures integrating electro-mechanical systems in order to optimize their vibro-acoustic behavior over a large frequency band and introduced a Floquet-Bloch decomposition for the computation of dispersion of two-dimensional periodic, damped mechanical systems [7].

Many physical systems in several scientific domains such as materials, acoustics, optics, mechanics, MEMS and vibrations can be modeled as periodic chain. Complex phenomenon such as solitary wave [8–10], discrete breathers [11, 12], wave localization emerged the trend to study the wave propagation in nonlinear periodic media. Chakraborty *et al.* [13] investigated the effects of harmonic wave propagation in an infinite, weakly nonlinear periodic chain. Romeo *et al.* [14] investigated analytically the modification of the boundary of linear propagation/attenuation zones due to the nonlinearities in chain of coupled oscillators, they also used the nonlinear propagation region of chain of oscillators with cubic nonlinearity exhibiting existence solutions to identify regions of existence of discrete breathers and to guide their analysis [15]. These nonlinearities can be due to the interaction between periodic structure and its neighbors. For instance, in the field of acoustics, Manktelow *et al.* [16, 17] focused on the interaction of wave propagation and analyzed the wave-wave interaction in a cubically nonlinear mono-atomic chain, while Marathe *et al.* [18] studied wave attenuation in nonlinear periodic structures. Lazarov *et al.* [19] focused on the influence of nonlinearities on the filtering properties of one-dimensional chain around the linear natural frequency of the attached nonlinear local oscillators. Boechler *et al.* [20] applied a straight-forward perturbation analysis, to a discrete one-dimensional nonlinear periodic chain with dynamics governed by a Hertzian contact model to obtain closed-form amplitude dependent dispersion relations and described the dynamic behavior of nonlinear periodic structures, along with how such structures can be utilized to affect the propagation of mechanical waves [21]. In Optics, Heinrich *et al.* [22] investigated the collective nonlinear dynamics in arrays of coupled optomechanical cells and Slusher *et al.* [23] introduced a vision of light controlling light in periodic photonic structures. Moreover, in micro and nanotechnology, dynamic behavior investigations of an array of N nonlinearly coupled microbeams have been performed by Gutschmidt *et al.* [24] using a continuum model and by Lifshitz *et al.* [25] using a discrete model.

Following this context, several authors analyzed the nonlinear dynamics of coupled structures, in the presence of a single excitation. Nayfeh *et al.* [26, 27] and Lifshitz *et al.* [28] studied parametrically excited multi-degree-of-freedom systems with different nonlinearities while Perkins *et al.* [29] illustrated the beneficial effects that noise can produce on the responses of an array of coupled nonlinear oscillators externally excited. However few studies have been devoted to simultaneous resonances [30–32] and they are mostly limited to single or few degree-of-freedom systems.

In this paper, we investigate a generic discrete model for the collective dynamics of periodic structures of coupled Duffing-Van Der Pol (VDP) oscillators, under simultaneous

primary and parametric resonances, which is suitable for several physical applications. The main goal is to understand how nonlinearities influence the presence of simultaneous external and parametric excitations and how they may be used to enhance and control modal interaction and bifurcation topology transfer between coupled oscillators. The analytical-computational model is based on the method of multiple scales coupled with standing wave modal decomposition, transforming the nonlinear differential system into a set of coupled complex algebraic equations which are numerically solved using the asymptotic numerical method (ANM) [33] enabling the construction of resonance curves for a large number of degree-of-freedom. The cases of small resonator arrays have been analyzed in the frequency domain and it is shown that the multi-mode solutions are stable over a wide frequency-range for a particular set of design parameters. The complexity and the multivaludness of the response were illustrated by a detailed study of its basins of attraction which prove theoretically the robustness of the multi-mode branches.

2 Model

2.1 Equation of motion

The proposed model involves a finite degree of linearly and nonlinearly coupled Duffing-VDP Oscillators, under primary and parametric excitations, as shown in Figure 1.

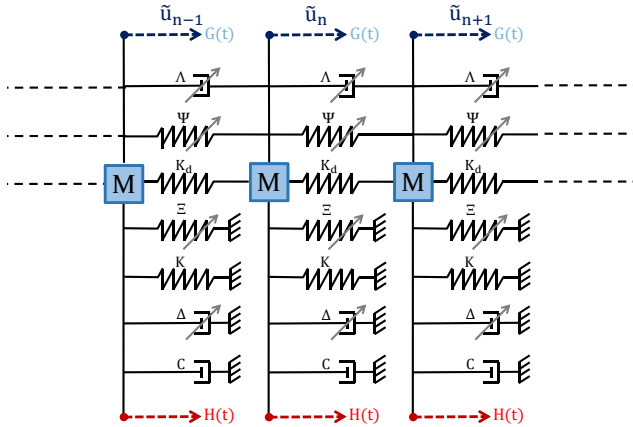


Fig. 1 A periodic nonlinear system of $N+2$ coupled Duffing-VDP oscillators, under simultaneous primary and parametric excitations.

The corresponding set of coupled equations of motion EOM can be written in the following form:

$$\begin{aligned}
 & M\ddot{u}_n - K_d(\tilde{u}_{n+1} - 2\tilde{u}_n + \tilde{u}_{n-1}) + C\dot{u}_n + K\tilde{u}_n \\
 & + \Psi[(\tilde{u}_n - \tilde{u}_{n+1})^3 + (\tilde{u}_n - \tilde{u}_{n-1})^3] + \Delta\tilde{u}_n^2\dot{\tilde{u}}_n + \Xi\tilde{u}_n^3 \\
 & + \Lambda[(\tilde{u}_n - \tilde{u}_{n+1})^2(\dot{\tilde{u}}_n - \dot{\tilde{u}}_{n+1}) + (\tilde{u}_n - \tilde{u}_{n-1})^2(\dot{\tilde{u}}_n - \dot{\tilde{u}}_{n-1})] \\
 & + H \cos[2\omega_0(1 + \varepsilon\Omega_D)t]\tilde{u}_n = G \cos[\omega_0(1 + \varepsilon\Omega_D)t]
 \end{aligned} \tag{1}$$

where \tilde{u}_n describes the deviation of the n^{th} resonator from its equilibrium $n = 0, \dots, (N+1)$, with fixed boundary conditions $\tilde{u}_0 = \tilde{u}_{N+1} = 0$. Ω_D and ω_0 are respectively the detuning parameter and the natural frequency of the oscillators. M is its effective mass, $K = M\omega_0^2$ is its effective spring constant, Ξ and Ψ are respectively the nonlinear stiffness and the coupling Duffing parameters, $C = \frac{M\omega_0}{Q}$ is the linear damping (Q is the quality factor), $K_d = \Gamma K$ is the coupling spring constant, Δ and Λ are respectively the VDP damping and the nonlinear dissipative coupling. H and G are the parametric and external excitation amplitudes respectively and ε is a small non-dimensional parameter.

2.2 Normalization

For convenience and equation simplicity, we introduce the nondimensional variables:

$$u_n = \frac{\tilde{u}_n}{\tilde{u}_D}, \quad t = \tilde{t}\omega_0 \quad (2)$$

where $\tilde{u}_D = \frac{G}{C\omega_0}$ is the dynamic displacement of the associated linear system while neglecting the linear coupling.

Substituting Equation (2) into the EOM, we obtain after dividing by $\frac{M\omega_0}{C}$

$$\begin{aligned} & \ddot{u}_n - \Gamma(u_{n+1} - 2u_n + u_{n-1}) + \frac{1}{Q}\dot{u}_n + u_n \\ & + \Psi[(u_n - u_{n+1})^3 + (u_n - u_{n-1})^3] + \delta u_n^2 \dot{u}_n + \xi u_n^3 \\ & + \lambda[(u_n - u_{n+1})^2(\dot{u}_n - \dot{u}_{n+1}) + (u_n - u_{n-1})^2(\dot{u}_n - \dot{u}_{n-1})] \\ & + \frac{H}{K} \cos[2(1 + \varepsilon\Omega_D)t]u_n = \frac{C}{M\omega_0} g \cos[(1 + \varepsilon\Omega_D)t] \end{aligned} \quad (3)$$

The parameters appearing in Equation (3) are:

$$\frac{\Delta G^2}{MC^2\omega_0^3} = \delta, \quad \frac{\Psi G^2}{MC^2\omega_0^4} = \psi, \quad \frac{\Xi G^2}{MC^2\omega_0^4} = \xi, \quad \frac{\Lambda G^2}{MC^2\omega_0^3} = \lambda. \quad (4)$$

We proceed in the following section to solve these coupled equations using secular perturbation theory. The linear damping coefficient is the physical parameter that allows us to use this approach. We therefore assume it to be small, by expressing it as $\frac{1}{Q} = \varepsilon\eta$ treating ε as a small expansion parameter. This limit is well verified for targeted applications where $Q \geq 50$ [28,34]. We also require that the Duffing and Van-Der-Pol nonlinearities to be a factor of ε smaller than the linear force, or equivalently by taking the leading order in u_n to be of the order of $\varepsilon^{\frac{1}{2}}$, and expressing $\Gamma = \frac{1}{2}\varepsilon\gamma$. In addition, we choose to take the parametric excitation amplitude to scale as the damping, i.e. we set $\frac{H}{K} = \varepsilon h$. To ensure that the external excitation g has the ability to cause such weak oscillations by having it enter the system at the same order as the physical effects, we write the amplitude of the drive as $\frac{C}{M\omega_0} = \varepsilon^{\frac{3}{2}}g$. On the other hand, u_n is proportional to GQ for a regular linear resonance, with u_n to be of order $\varepsilon^{\frac{1}{2}}$ and Q , of order ε^{-1} thus G has to be of order $\varepsilon^{\frac{3}{2}}$.

2.3 Derivation of the amplitude equation

We expand $u_n(t)$ as a sum of standing-wave modes with slowly varying amplitudes [28]:

$$u_n(t) = \varepsilon^{\frac{1}{2}} \sum_{m=1}^N (A_m(T) \sin(nq_m) e^{i\omega_m t} + c.c.) + \varepsilon^{\frac{3}{2}} u_n^{(1)}(t) + \dots, \quad n = 1, \dots, N, \quad (5)$$

where $T = \varepsilon t$ is a slow time variable, that authorizes the complex amplitude $A_m(T)$ to vary slowly in time. Since the boundary conditions are such that there are two additional fixed masses labeled 0 and $N+1$ ($u_0 = u_{N+1} = 0$), the possible wave components q_m are given by

$$q_m = \frac{m\pi}{N+1}, \quad m = 1, \dots, N \quad (6)$$

After replacing the equations listed in Appendix A into the EOM, we can get at the order of $\varepsilon^{\frac{3}{2}}$, N equations of the form:

$$\ddot{u}_n^{(1)} + u_n^{(1)} = \sum_m (m^{th} \text{ secular term}) e^{i\omega_m t} + \text{other terms}$$

On the right hand side, we have N secular terms that act to drive the coupled oscillators $u_n^{(1)}$ at their resonance frequencies. We require them to be vanished so that $u_n^{(1)}$ remain finite, and thus we obtain the equations for the slowly varying amplitudes $A_m(T)$. To extract the equation for the m^{th} amplitude $A_m(T)$, we make use of the orthogonality of the modes, by multiplying the m^{th} secular term by $\sin(nq_m)$ and summing over n . We also express all normal frequencies relative to 1, so that:

$$\omega_m = 1 + \varepsilon \Omega_m \quad (7)$$

We find that the equation of the m^{th} amplitude $A_m(T)$ is given by:

$$\begin{aligned} 2i\omega_m \frac{dA_m}{dT} + 2\gamma\omega_m \sin^2\left(\frac{q_m}{2}\right)A_m + \frac{h}{2}A_m^* e^{2i(\Omega_D - \Omega_m)T} + i\omega_m \eta A_m \\ + \frac{1}{4} \sum_{j,k,l} R_k \{i\omega_l \delta[2R_{j,l} - R_{j,l}^*] + 3\xi R_{j,l}^*\} \Delta_{jkl,m}^{(1)} \\ + 4 \sin\left(\frac{q_m}{2}\right) \sum_{j,k,l} R_k \{3\psi R_{j,l}^* + i\omega_l \lambda [2R_{j,l} - R_{j,l}^*]\} \Pi_{j,k,l} \Delta_{jkl,m}^{(2)} \\ = \frac{g}{(N+1)} e^{i(\Omega_D - \Omega_m)T} \sum_{n=1}^N \sin(nq_m), \end{aligned} \quad (8)$$

with $R_k = A_k e^{i(\Omega_k - \Omega_m)T}$ and $R_{j,l} = A_j^* A_l e^{i(-\Omega_j + \Omega_l)T}$, where we have introduced two Δ functions, defined in Appendix B.

Ignoring initial transients, and assuming that the nonlinear terms in the equation are sufficient to saturate the growth of the instability, we try a steady-state solution of the form

$$A_m = a_m e^{i[\Omega_D - \Omega_m]T} \quad (9)$$

Substituting Equation (9) into Equation (8) of amplitude, we obtain the required equation for the fixed complex amplitudes a_m .

$$\begin{aligned}
& [i\eta - 2(\Omega_D - \Omega_m)]\omega_m a_m + 2\gamma \sin^2\left(\frac{q_m}{2}\right)a_m + \frac{h}{2}a_m^* \\
& + \frac{1}{4} \sum_{j,k,l} [i\omega_l \delta(2a_j^* a_k a_l - a_j a_k a_l^*) + 3\xi a_j a_k a_l^*] \Delta_{jkl,m}^{(1)} \\
& + 4 \sin\left(\frac{q_m}{2}\right) \sum_{j,k,l} \Pi_{j,k,l} \left[3\psi a_j a_k a_l^* \right. \\
& \left. + i\omega_l \lambda (2a_j^* a_k a_l - a_j a_k a_l^*) \right] \Delta_{jkl,m}^{(2)} \\
& = \frac{g}{(N+1)} \sum_{n=1}^N \sin(nq_m)
\end{aligned} \tag{10}$$

Equation (10) is a complex algebraic system, with large number of variables. Analytical solutions for this type of equations are either too large or simply do not exist. As a first step, we choose to simplify these equations by setting the reference frequencies ω_m to be 1, by taking $\Omega_m = 0$. In this case, the only possibility is to solve it numerically, using a conventional method. Mathematica can be used to solve the system for two coupled oscillators, including stability analysis. This method is based on prediction-correction algorithms, such as the Newton-Raphson scheme which is the most popular way to solve a nonlinear structural problem. In general such algorithms are successful for determining nonlinear solution branches in a step-by-step manner, with a load control, a displacement control or an arc length control but they have two disadvantages: The first one, is that they are time-consuming comparing to a linear problem and the second one is the automatization of the continuation process.

Therefore, a graphical interactive software named MANLAB [35] has been used for the continuation of branches of solutions of Equations (10) by an alternative method, which is called the Asymptotic Numerical Method (ANM) [33,36]. The ANM can be considered as an extension of methods of type prediction-correction, where the tangent predictor is replaced by a high-order predictor, where we solve an important number of linear systems for each prediction. The main constraint of this method is to write the algebraic equations of the form $R(U) = 0$, where U is a vector of $n + 1$ unknowns and R a vector of n smooth equations that must be analytical. The ANM is a perturbation technique which consists in expanding the unknown vector U as a formal power series of a path parameter. It presents several advantages: it provides continuous solutions, the continuation is very robust, and the control of the step length is automatic and always optimal. MANLAB provides linear stability analysis for equilibrium points of dynamical systems with an automatic Bifurcation detection. This method and its application to our nonlinear differential system (8) is detailed here after.

2.4 Cartesian transformation

To use the ANM, Equation (8) is transformed to its Cartesian form by defining the amplitude as $A_m = (\alpha_m + i\beta_m)e^{i\Omega_D T}$. As a result, we obtain the following general equations, for which the unknowns are real:

$$\begin{aligned}
\alpha'_m(T) = & -\frac{\eta}{2}\alpha_m + \Omega_D\beta_m + \frac{h}{4}\beta_m - \gamma\sin\left[\frac{q_m}{2}\right]^2\beta_m \\
& -\frac{1}{8}\sum_{j,k,l}\left[\delta(\alpha_j\alpha_k\alpha_l + \alpha_j\beta_k\beta_l)\right. \\
& \left.+ 3\xi(\alpha_j\alpha_k\beta_l + \beta_j\beta_k\beta_l)\right]\Delta_{jkl,m}^{(1)} \\
& -2\sin\left[\frac{q_m}{2}\right]\sum_{j,k,l}\Pi_{j,k,l}\left[\psi(\alpha_j\alpha_k\alpha_l + \alpha_j\beta_k\beta_l)\right. \\
& \left.+ 3\lambda(\alpha_j\alpha_k\beta_l + \beta_j\beta_k\beta_l)\right]\Delta_{jkl,m}^{(2)}
\end{aligned} \tag{11}$$

and

$$\begin{aligned}
\beta'_m(T) = & -\frac{\eta}{2}\beta_m - \Omega_D\alpha_m + \frac{h}{4}\alpha_m + \gamma\sin\left[\frac{q_m}{2}\right]^2\alpha_m \\
& -\frac{g}{2(N+1)}\sum_{n=1}^N\sin(nq_m) - \frac{1}{8}\sum_{j,k,l}\left[3\xi(\alpha_j\alpha_k\alpha_l + \alpha_j\beta_k\beta_l)\right. \\
& \left.-\delta(\alpha_j\alpha_k\beta_l + \beta_j\beta_k\beta_l)\right]\Delta_{jkl,m}^{(1)} \\
& -2\sin\left[\frac{q_m}{2}\right]\sum_{j,k,l}\Pi_{j,k,l}\left[3\psi(\alpha_j\alpha_k\alpha_l + \alpha_j\beta_k\beta_l)\right. \\
& \left.-\lambda(\alpha_j\alpha_k\beta_l + \beta_j\beta_k\beta_l)\right]\Delta_{jkl,m}^{(2)}
\end{aligned} \tag{12}$$

The steady-state motions occur when $\alpha'_m = \beta'_m = 0$, which corresponds to the singular points of Equations (11) and (12). With these two equations, the stability of fixed points is easy to implement.

2.5 Quadratic recast

The key point of the ANM lies in the quadratic recast of Equations (11) and (12) by introducing the following set of auxiliary variables,

$$\begin{aligned}
\alpha_i^2 &= c_i & \text{size } N \\
\beta_i^2 &= d_i & \text{size } N \\
\alpha_i\alpha_j &= e_{i,j} \text{ for } i \neq j & \text{size } \frac{N(N-1)}{2} \\
\beta_i\beta_j &= f_{i,j} \text{ for } i \neq j & \text{size } \frac{N(N-1)}{2}.
\end{aligned} \tag{13}$$

These transformations lead to the following quadratic system

$$R(\mathbf{U}) = L_0 + L(\mathbf{U}) + Q(\mathbf{U}, \mathbf{U}) = 0 \tag{14}$$

where \mathbf{R} is a vector of $N^2 + 3N$ equations and $\mathbf{U} = (\boldsymbol{\alpha}, \boldsymbol{\beta}, \mathbf{c}, \mathbf{d}, \mathbf{e}, \mathbf{f}, \Omega_D)^T$ is the vector of $N^2 + 3N + 1$ unknowns, in which $\boldsymbol{\alpha}, \boldsymbol{\beta}, \mathbf{c}, \mathbf{d}, \mathbf{e}$ and \mathbf{f} are vectors, as

$$\begin{aligned}
 \boldsymbol{\alpha} &= \{\alpha_1, \alpha_2, \dots, \alpha_i, \dots, \alpha_N\} \\
 \boldsymbol{\beta} &= \{\beta_1, \beta_2, \dots, \beta_i, \dots, \beta_N\} \\
 \mathbf{c} &= \{c_1, c_2, \dots, c_i, \dots, c_N\} \\
 \mathbf{d} &= \{d_1, d_2, \dots, d_i, \dots, d_N\} \\
 \mathbf{e} &= \{e_{1,2}, e_{1,3}, \dots, e_{1,N}, \dots, e_{i,i+1}, \dots, e_{i,N}, \dots, e_{N-1,N}\} \\
 \mathbf{f} &= \{f_{1,2}, f_{1,3}, \dots, f_{1,N}, \dots, f_{i,i+1}, \dots, f_{i,N}, \dots, f_{N-1,N}\}
 \end{aligned} \tag{15}$$

L_0 is a constant vector, $L(\cdot)$ and $Q(\cdot)$ are respectively the linear and quadratic operators with respect to \mathbf{U} .

2.6 Stability analysis

Different algorithms are implemented in ManLab [35] in order to analyze the linear stability of dynamical systems. Two stability computation methods are proposed depending on the type of the solution under study and on the selected algorithm: frequency domain or Time-domain. The latter has been used to analyze the stability of fixed points in order to identify the stable multi-mode solution branches. Therefore, To analyze the linear stability of the dynamical systems, the time-domain algorithm is used. This algorithm relies on the computation of the Jacobian matrix J , of Equations (11) and (12). The linear stability analysis consists in computing the eigenvalues of the Jacobian matrix at each point of analysis. If any of the eigenvalues has a positive real part, then the current point is unstable. When following a branch that is, at first stable, a bifurcation can be detected when one of the eigenvalues crosses the imaginary axis. This analyze uses three additional functions J_0 , JL and JQ as

$$J = J_0 + JL + JQ \tag{16}$$

where J_0 is a constant matrix, JL is a linear operator and JQ a quadratic operator on the variables given in $\mathbf{U}_{stab} = \{\boldsymbol{\alpha}, \boldsymbol{\beta}, \Omega_D\}$ which is the variables vector of size $N^2 + 1$. From a practical point of view, one can easily recast the equations of motion of nonlinear periodic structures with respect to the proposed model and hence one can use the procedure detailed above as a robust solving tool.

3 Results and discussions

In order to target various periodic structure-based systems, the numerical simulations have been performed with two sets of design parameters listed in Table 1. The first one contains the Duffing coupling term and the nonlinear damping for each oscillator while the second one involves the VDP coupling and the nonlinear cubic stiffness. Indeed, the two configurations can illustrate respectively an array of coupled levitated magnets [37] and a periodic structure of coupled micro or nano-beams[28]. Moreover, the external excitation G has been chosen sufficiently high in order to generate nonlinear frequency responses for which the displacement at resonance is beyond the critical Duffing amplitude [38], while the value of the parametric excitation H has been adjusted in order to increase the interactions between both resonances (primary and parametric) and enrich the resulting collective dynamics.

Table 1 Design parameters for the corresponding periodic structure depicted in Figure 1

Parameters	Design 1	Design 2
$c(Kg.s^{-1})$	0.001	0.01
$M(Kg)$	0.01	0.01
$K(N.m^{-1})$	40	40
$\Delta(Kg.m^{-2}.s^{-1})$	50	0
$\Psi(N.m^{-3})$	5000	0
$\Xi(N.m^{-3})$	0	800
$\Lambda(Kg.m^{-2}.s^{-1})$	0	6
Γ	0.001	0.001

3.1 Case of two coupled nonlinear resonators

As a first step, we started by solving the coupled Equations (10) with $N = 2$ for the first design, in order to provide some qualitative and quantitative explanations dealing with the collective nonlinear dynamics of small arrays of periodic structures which can be extended for large periodic lattices. For two coupled oscillators, we have:

$$q_1 = \frac{\pi}{3} \quad \text{and} \quad q_2 = \frac{2\pi}{3}.$$

The coupled algebraic equations have been solved numerically using Mathematica, for several values of Ω_D inside the frequency range where the whole dynamic response is represented and the stability of the different branches have been performed based on the eigen values of the Jacobian matrix of the differential system (8) computed numerically for each point.

3.1.1 Primary resonance

In this section, we are interested in the collective nonlinear dynamics of the coupled oscillators under primary resonance ($G = 0.08$). By solving numerically the resulting system, the overall collective response of the array can be plotted with respect to the detuning parameter Ω_D . With two resonators, there are regions in frequency where three stable solutions can exist. The single mode (SM) of the first intensity corresponds to the forced frequency response of a single Duffing oscillator, and for the second one to a null trivial solution. Remarkably, the double mode (DM) contains two added stable branches as we can see in Figures 2 (a) and (b). By zooming over a precise frequency range, we can easily remark that we have a modal interaction and bifurcation topology transfer between these two coupled oscillators. Although, these branches are stable, it is hard to reach them experimentally, because their basins of attraction are very narrow. Consequently we extend the investigations to the case of simultaneous primary and parametric excitations, seeking for additional properties.

3.1.2 Simultaneous primary and parametric resonances

In order to illustrate the complexity of the collective dynamics for the considered periodic structure, the case of simultaneous resonances is numerically investigated for $G = 0.1$ and $H = 7$. Figure 3 displays the intensity responses, as a function of the detuning parameter Ω_D and remarkably, for the first intensity response, an elliptical branch was added due to the parametric excitation.

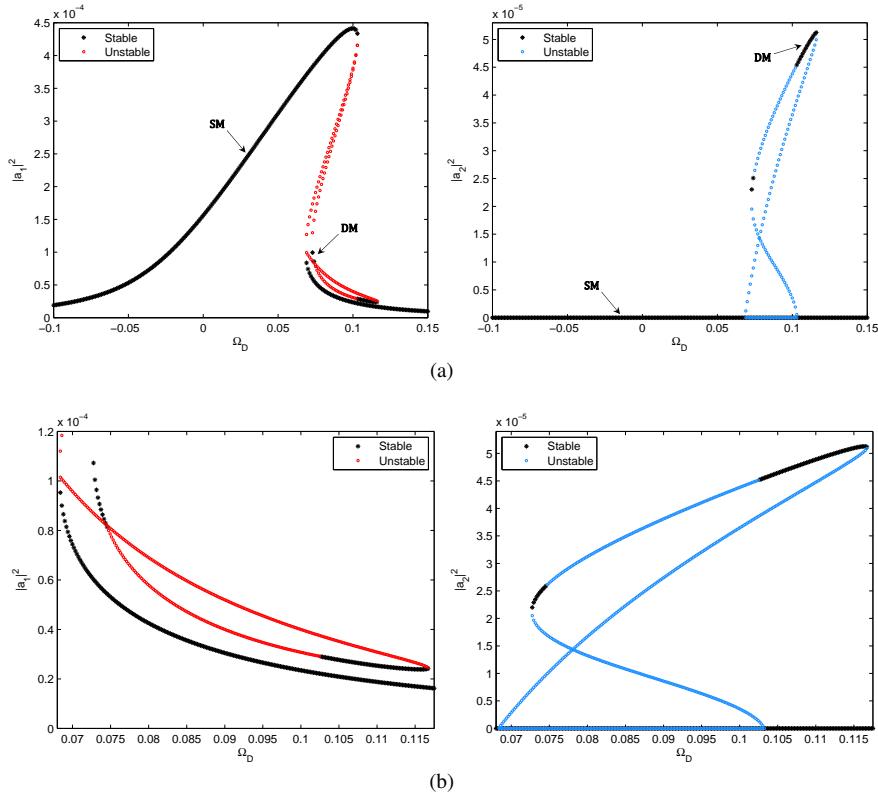


Fig. 2 (a) Response intensity of two resonators as a function of the detuning parameter Ω_D , under primary resonance ($G = 0.08$), for the first design parameters. (b) Zooming in and highlighting the responses areas. Black curves indicate stable solutions. The Single and Double-Mode solution branches are labeled SM and DM respectively.

In addition, with a small change in the excitation amplitudes ($G = 0.08$ and $H = 11$), we can obtain up to four solutions for a given frequency for the first intensity response, as shown in Figure 4. The frequency response plotted in Figure 5, represents the time and space average of the square of the oscillator displacement.

$$I = \frac{1}{N} \sum_{n=1}^N \langle u_n^2 \rangle, \quad (17)$$

where the angular brackets denote time average, using the fact that for $N = 2$, $I = \frac{3}{2}(|a_1|^2 + |a_2|^2)$. The multivaluedness of the response curve due to the nonlinearity has a significance from the physical point of view because it leads to jump phenomena which are localized at the bifurcation points. In addition, the DM has an important amplitude and its stable over a wide frequency range, which implies significant modal interactions due to nonlinearities.

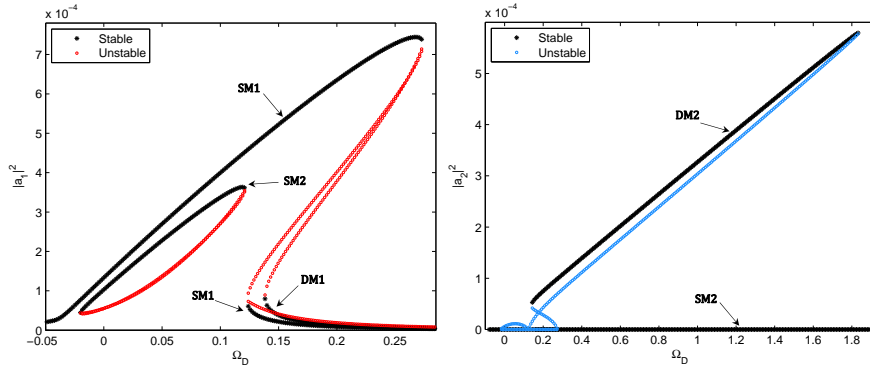


Fig. 3 Response intensity of two coupled oscillators as a function of the detuning parameter Ω_D , under simultaneous primary and parametric resonances ($G = 0.1, H = 7$), for the first design parameters. The Single and Double-Mode solution branches are labeled SM i and DM i respectively, with $i \in \{1, 2\}$

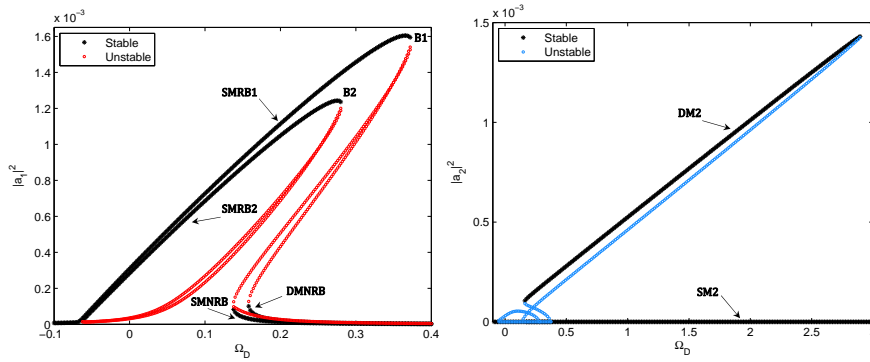


Fig. 4 Response intensity of two coupled oscillators as a function of the detuning parameter Ω_D , under simultaneous primary and parametric resonances ($G = 0.08, H = 11$), for the first design parameters. SMRB1 and SMRB2 are Single Mode Resonant Branches due respectively to primary and parametric resonances. SMNRB and DMNRB are respectively Single and Double Mode Non Resonant Branches.

3.2 Basins of attraction

The basins of attraction can be used for qualitative as well as quantitative analysis of the collective dynamics robustness. In a nonlinear nanomechanical resonator, Kozinsky *et al.* [39] experimentally probe the basins of attraction of two fixed points. Moreover, Sliwa *et al.* [40] investigated the basins of attraction of two coupled Kerr oscillators. Furthermore, Ruzziconi *et al.* [41] studied frequency response curves, behavior charts and attractor-basins phase portraits of a considered NEMS constituted by an electrically actuated carbon nanotube.

In this section, the basins of attraction are used to investigate qualitatively as well as quantitatively the trajectories of the system response, the robustness of the attractors and their practical implications, for the case of two coupled Duffing-VDP oscillators under simultaneous primary and parametric resonances. The analyzes are performed in a classical way where the robustness is only related to the global size of the attractor. Although the basins of attraction are usually plotted in the phase plane (u_n, \dot{u}_n) , we choose to represent them in different diagrams for convenience regarding the adopted solving procedure leading

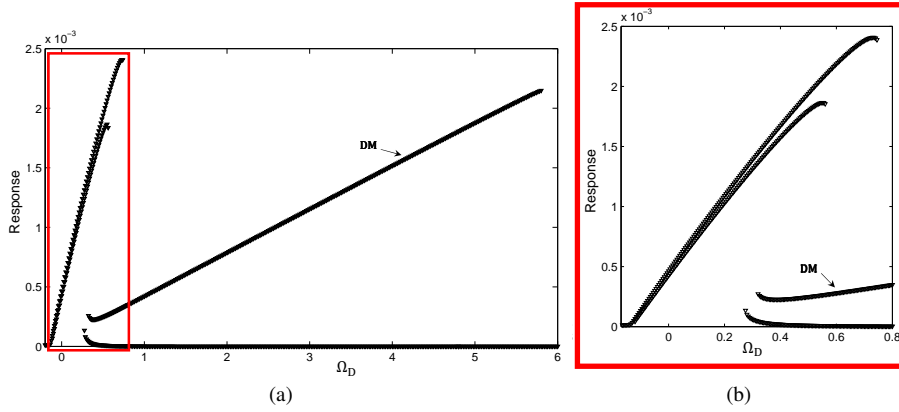


Fig. 5 (a) Averaged response intensity defined in Equation 17. (b) Zooming and highlighting over a region which contains up to four stable solutions. Branch labels correspond to those in Figure 4.

to the differential Equations (11) and (12). The initial conditions $\alpha_i(0)$ and $\beta_i(0)$ have been bounded by $-|a_i|$ and $|a_i|$ which can be identified on the response intensity curves.

As a first step, the case $\Omega_D = 0.255$ is considered. It corresponds to a multistable response with four attractors for the first intensity and two for the second one. Figures 6 (a) and (b) display the basins of attraction plotted respectively in the planes $(\alpha_1(0), \alpha_2(0))$ for $\beta_1(0) = \beta_2(0) = 0$ and $(\beta_1(0), \beta_2(0))$ with $\alpha_1(0) = \alpha_2(0) = 0$. Remarkably, these curves show that the basins of attraction are symmetric with respect to $\alpha_2(0) = 0$ and $\beta_2(0) = 0$ and thus, one can investigate their distribution in the Nyquist plane $(\alpha_1(0), \beta_1(0))$, while setting random positive values of $\alpha_2(0)$ and $\beta_2(0)$.

When the first response jumps between SMRB1, SMRB2 and SMNRB, the second one is stabilized on the SM and a similar correspondence exists between the double modes as shown in Figure 7. This results in an interesting transfer of basins of attraction topologies between both responses with respect to the type of branches described in Figure 4. Thus, one can restrict the analysis to the attractor robustness of the double mode of $|a_1|^2$.

Then, the basins of attraction of the first response are plotted in the Nyquist plane while varying the detuning parameter Ω_D to track the evolution of the attractor topology when the oscillators are going from a bistable to a multistable state, as shown in Figure 8. For instance, $|a_1|^2$ displays two stable resonant solutions for $\Omega_D = 0.07$. At the considered detuning parameter, the basins of attraction of SMRB1 are larger than those of SMRB2 due to the difference in the frequency distances separating the corresponding solutions and the bifurcations points B_1 and B_2 . For $\Omega_D = 0.16$, another stable solution is added, It is located on the non-resonant branch of the single mode and its basins of attraction take a small domain in the Nyquist plane as shown in Figure 8 (b).

The basins of attraction of the double mode take place in Figures 8 (c) and (d) and their size increases and becomes significantly large for $\Omega_D = 0.19$ with respect to the attractor size of the non-resonant branch which is almost null for $\Omega_D = 0.25$. Although these lower branches are very close as shown in Figure 4 for $|a_1|^2$, they do not have the same nature and this is proved regarding the frequency response of $|a_2|^2$, which justifies the large differences in their attractor topologies.

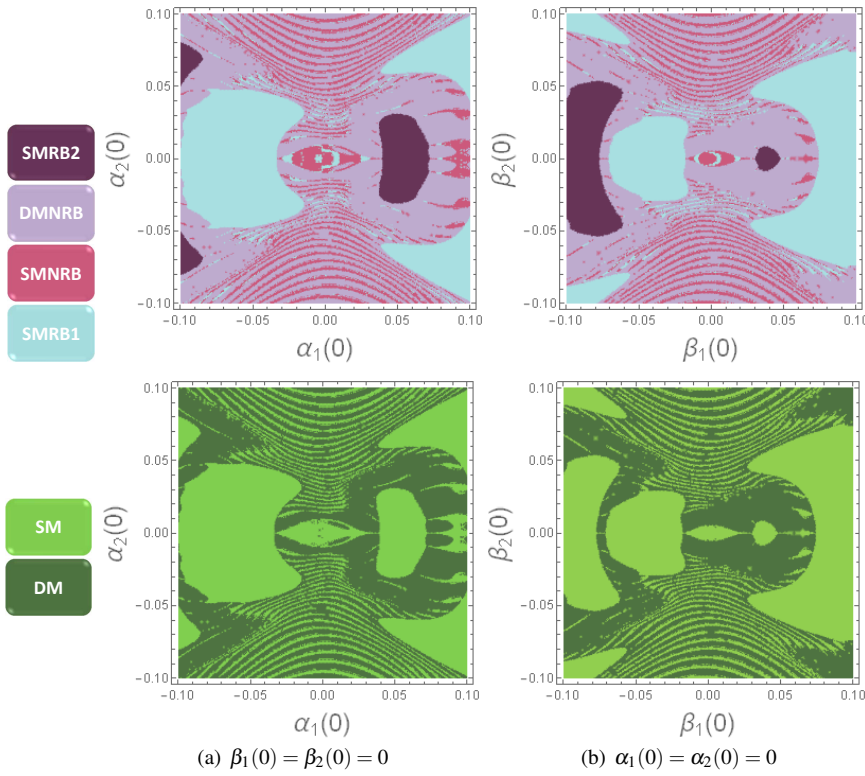


Fig. 6 Distribution of the basins of attraction for the two responses $|a_1|^2$ (at the top) and $|a_2|^2$ (in the bottom) for $\Omega_D = 0.255$ in the planes $(\alpha_1(0), \alpha_2(0))$ and $(\beta_1(0), \beta_2(0))$.

Figure 9 displays the distribution of the basins of attraction of $|a_1|^2$ in the Nyquist plane for $\Omega = 0.255$ and three different parametric excitation amplitudes. When H is decreased from 11 to 6.7, the number of stable solutions decreases for the considered detuning parameter at which it is not possible to intercept SMRB2. Indeed, a large part of the basins of attraction of SMRB2 for $H = 11$ is taken by the double mode for $H = 8.5$. Moreover, if we decrease the parametric excitation amplitude down to $H = 6.7$, the oscillator becomes bistable and can switch solution between the double mode and the non-resonant branch of the single mode. Nevertheless, the double mode is more robust, since its basins of attraction represent more than 50% of the whole domain of initial conditions. In practice, the attractor topology can be tuned with respect to the parametric excitation in order to enlarge the basins of attraction of the double mode and obtain an interesting collective dynamics very well adapted for nonlinear energy localization.

Finally, to prove the robustness of the double mode, a quantitative study has been made, based on a random sampling. It consists in solving sequentially the differential Equations (11) and (12) by allowing the initial conditions to be random at each iteration. Of 100 000 sampled initial conditions, the double mode occurs 47%. Interestingly, the basins of attraction of the double mode are large, which demonstrates the attractor robustness. Consequently, once functionalized in term of nonlinearity, the proposed periodic structure can be exploited for jumps-based sensing techniques [42].

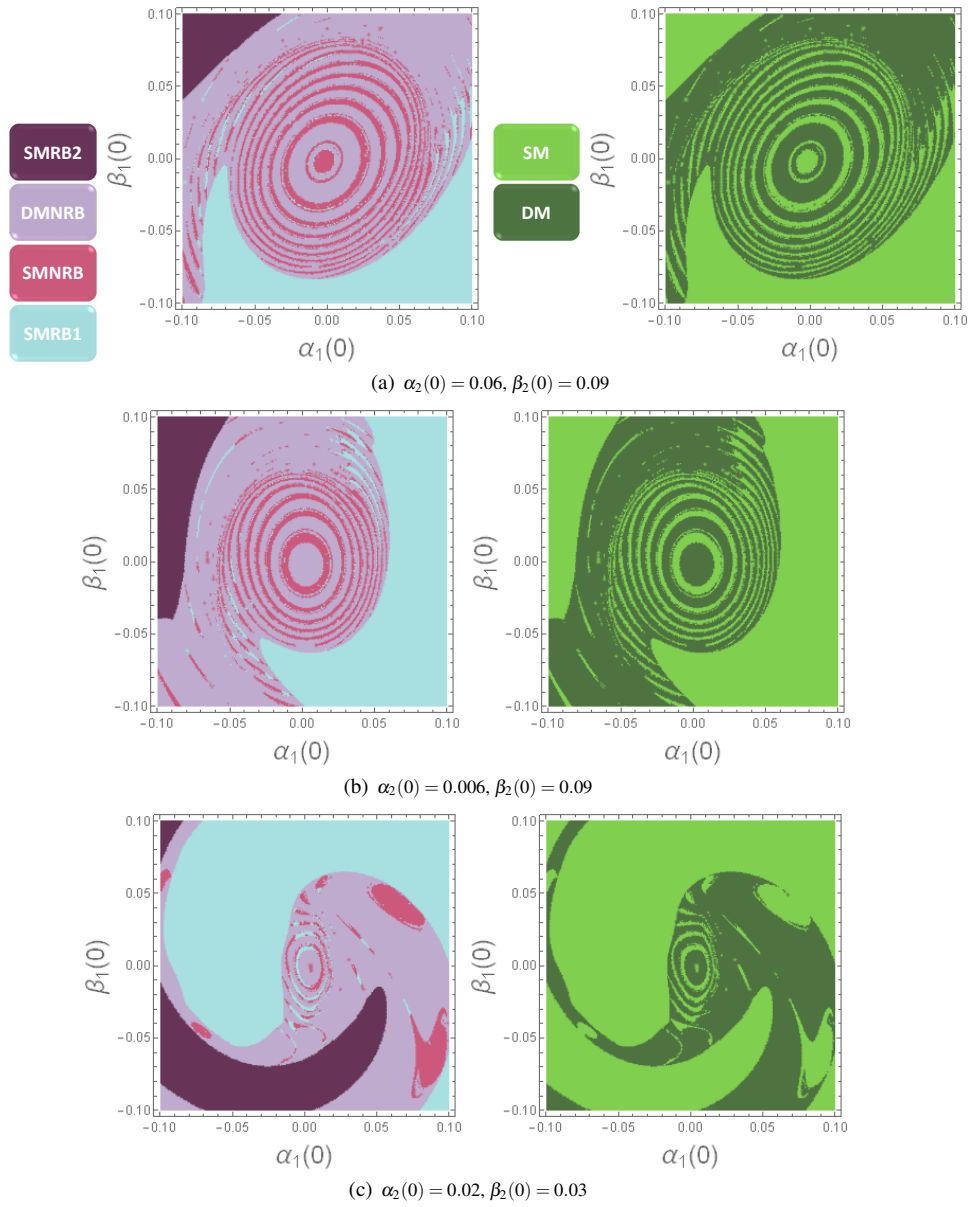


Fig. 7 Distribution of the basins of attraction for the two responses $|a_1|^2$ (on the left) and $|a_2|^2$ (on the right) in the Nyquist plane (α_1, β_1) , for a fixed detuning parameter $\Omega = 0.255$.

3.3 Case of three coupled nonlinear resonators

Figure 10 displays the response intensity of three coupled oscillators as a function of the detuning parameter Ω_D , under simultaneous parametric and external excitations ($H = 20$

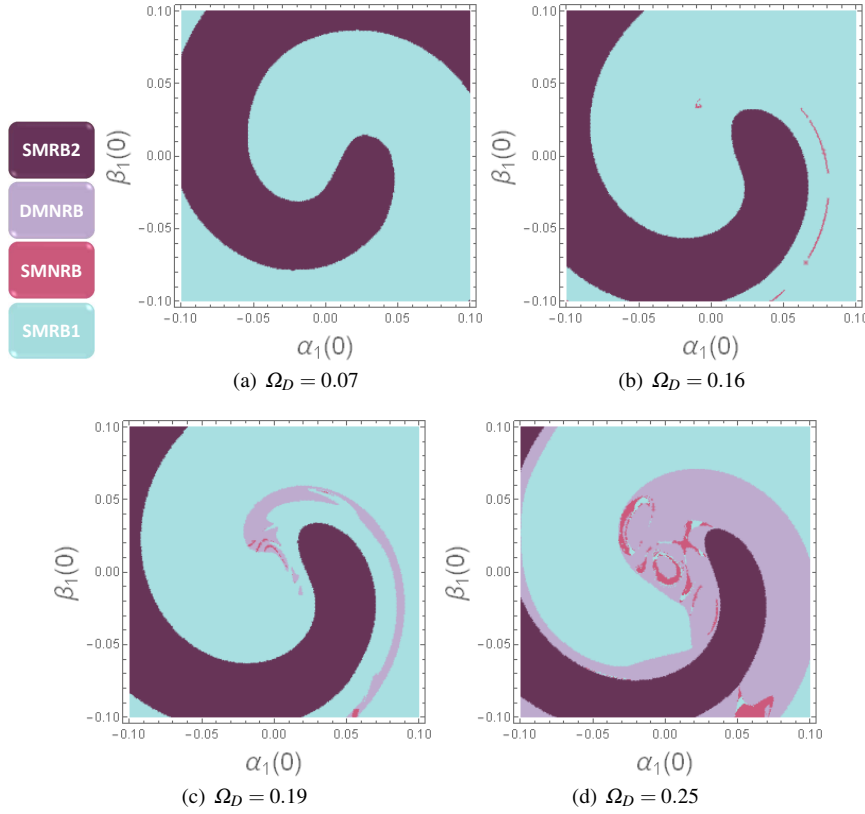


Fig. 8 Evolution of the basins of attraction for the first intensity response with $\alpha_2(0) = 0.01$, $\beta_2(0) = 0.02$ with respect to the detuning parameter in the Nyquist plane.

and $G = 0.4$), for the second set of design parameters given in Table 1. The curves show the squares of the amplitudes of the three different modes, where the only SM corresponds the trivial null solution of Equation (10), for $N = 3$ and $m = 2$. Remarkably, all solutions of $|a_1^2|$ and $|a_3^2|$ are multimodal. The Double and Triple mode solution branches, result from the coupling between the first and third oscillators, and the three coupled oscillators respectively. They are denoted by: Di_j and Tk_l for $i \in \{1, 3\}$, $j \in \{1, 2, 3, 4\}$ and $k, l \in \{1, 2, 3\}$. Thus, in this case the periodic structure is completely driven by the collective dynamics due to the modal interactions between the nonlinear oscillators. This is demonstrated in Figure 11, where we plotted the average response intensity, defined in Equation (17), which is $I = \frac{4}{3}(|a_1^2| + |a_2^2| + |a_3^2|)$ for $N = 3$.

In addition, it is noticeable that each bifurcation point due to a multi-modal solution on $|a_2|^2$ has a correspondence on the two other intensity responses (for instance, B_1 , B_2 and B_3), which proves that the bifurcation topology transfer is general for any number of oscillators. Moreover, there are multimode solution branches that are completely disconnected from all other branches. Among them, two Triple Mode solutions localized in the detuning interval $[-0.107, 0.007]$.

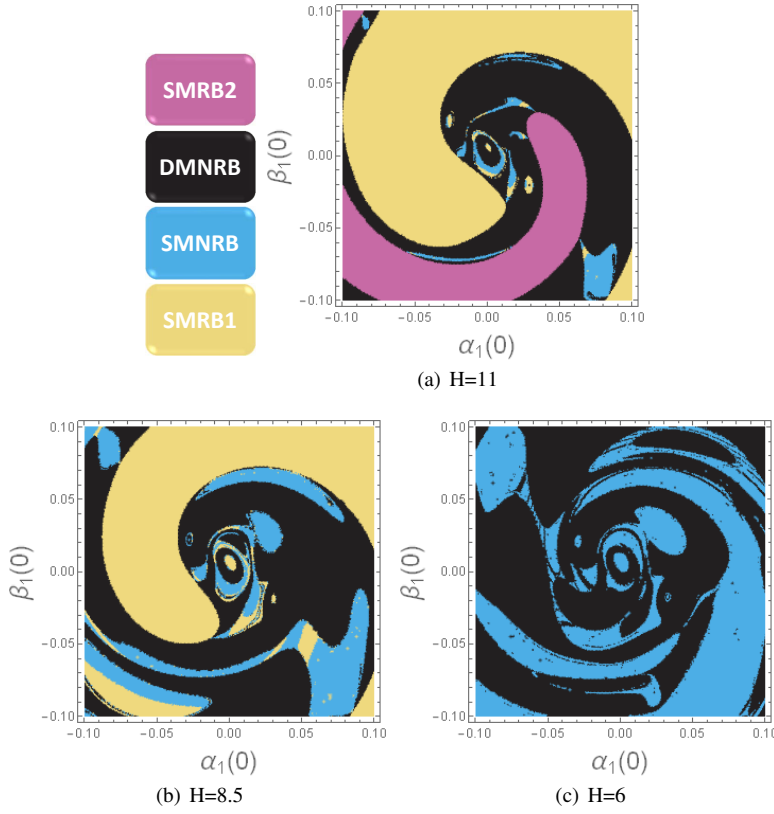


Fig. 9 Evolution of the basins of attraction for the first intensity response with $\alpha_2(0) = 0.05$, $\beta_2(0) = 0.02$ and $\Omega = 0.255$ with respect to the parametric excitation amplitude in the Nyquist plane.

These curves were plotted to underline the large number of solution branches even for a small number of coupled oscillators. Indeed, the intensity responses of $|a_1^2|$ and $|a_3^2|$ are highly multistable with up to seven stable non-trivial solutions for a given frequency (four double mode and three triple mode solutions). For the configuration, when $\Omega_D = 0.46$, the distributions of the basins of attraction for the three intensity responses are plotted in Figures 11 (a) and (b) in the Nyquist plane $(\alpha_1(0), \beta_1(0))$, for random initial conditions $\alpha_2(0) = 0.06$, $\beta_2(0) = 0.48$, $\alpha_3(0) = 0.38$ and $\beta_3(0) = 0.39$. We remark that $|a_1|^2$ and $|a_3|^2$ have the same basin distribution and a transfer of basins of attraction topology exists between the three oscillators with respect to the solution branch nature. Furthermore, the probability of reaching the triple mode solution branches is about 32% and their robustness can be adjusted with respect to the design parameters.

It is notable in basins of attraction Figures that most fractal parts are negligible with respect to the compact parts of the attractors which implies good agreements with the dynamical integrity of the system [43]. Nevertheless, for large arrays of oscillators, the fractal parts will increase due to the important number of multi-modal solution branches, and therefore, the dynamical integrity [44–46] must be analyzed by choosing the right definition of

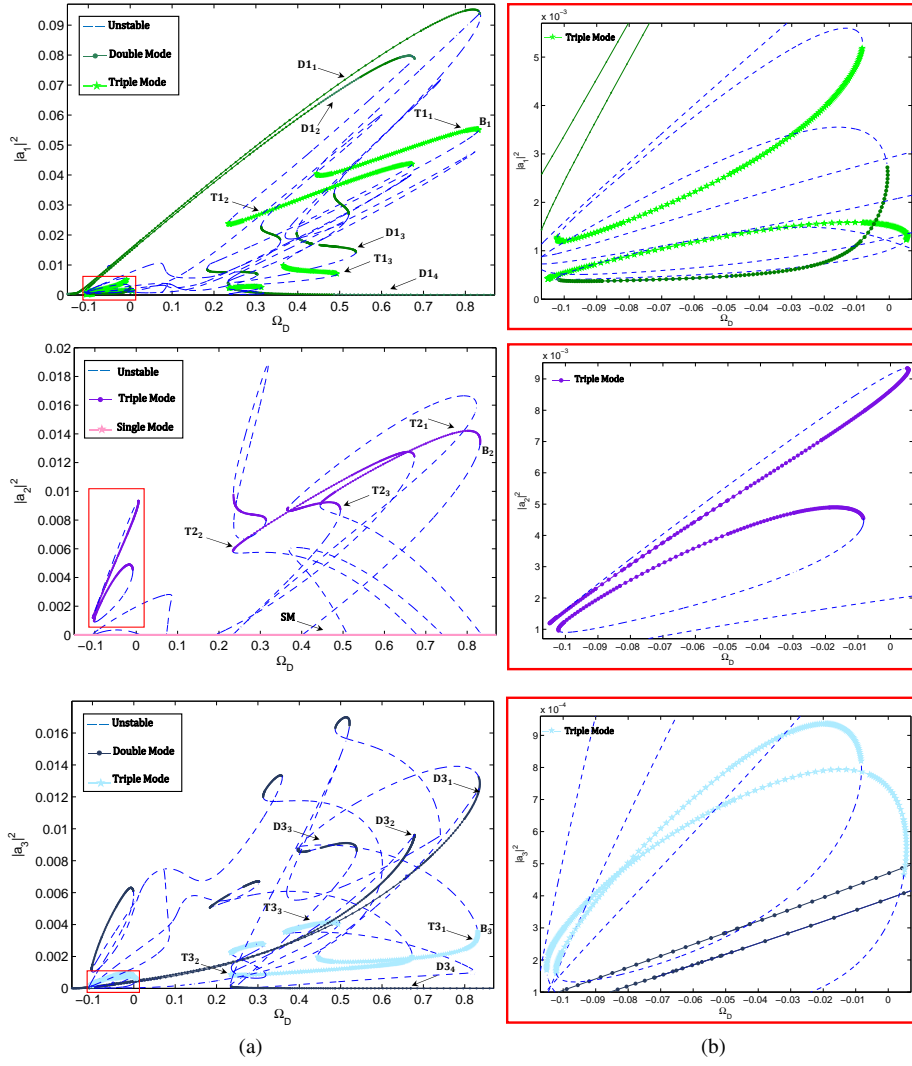


Fig. 10 (a) Response intensity of three coupled oscillators as a function of the detuning parameter Ω_D , under simultaneous primary and parametric resonances ($G = 0.4, H = 20$), for the second design parameters. The Double and Triple Mode solution branches are denoted by: Di_j and Tk_l for $i \in \{1, 3\}, j \in \{1, 2, 3, 4\}$ and $k, l \in \{1, 2, 3\}$ and respectively. The only Single Mode denoted by SM corresponds to the trivial null solution of Equation (10), for $N = 3$ and $m = 2$. (b) Zooming and highlighting over a region that contains multimode solution branches that are completely disconnected from all other branches.

safe basin, choosing an appropriate integrity measures to qualify its magnitude and investigating the basins evolution for varying system parameter.

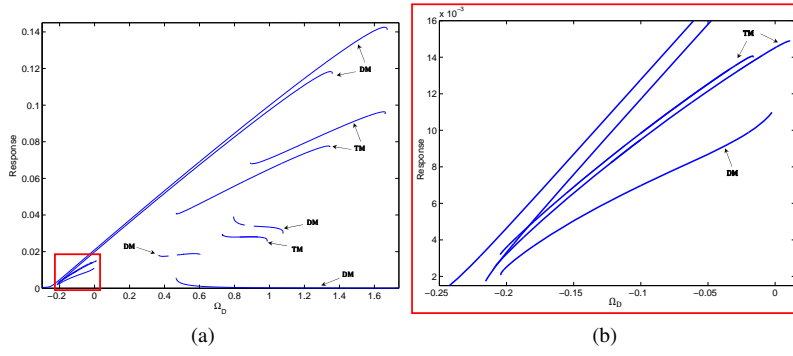
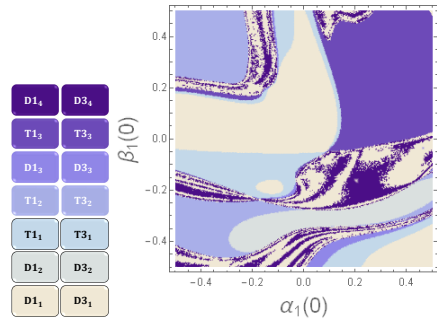
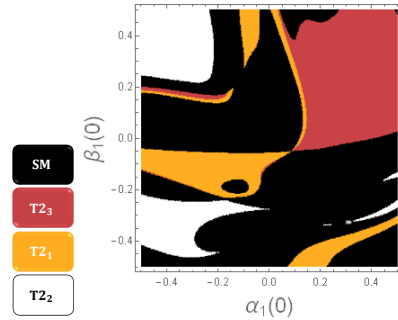


Fig. 11 (a) Averaged Response intensity defined in Equation (17). (b) zooming and highlighting over a region that contains up to five stable solutions. DM and TM denote the branches due to Double and Triple Modes respectively.



(a) Basins of attraction of $|a_1|^2$ and $|a_3|^2$.



(b) Basins of attraction of $|a_2|^2$.

Fig. 12 Distribution of the basins of attraction for the three responses $|a_1|^2, |a_2|^2$ and $|a_3|^2$ for $\Omega_D = 0.46$ in the Nyquist plane $(\alpha_1(0), \beta_1(0))$, with the random initial conditions $\alpha_2(0) = 0.06, \beta_2(0) = 0.48, \alpha_3(0) = 0.38$ and $\beta_3(0) = 0.39$.

4 Conclusion

The collective nonlinear dynamics of periodic nonlinear oscillators was modeled for specific discrete systems of coupled Duffing-VDP oscillators under simultaneous primary and para-

metric excitations. The model is hybrid combining analytical and computational methods and precisely based on the secular perturbation theory with the standing wave decomposition and the asymptotic numerical continuation technique. The cases of two and three coupled oscillators were investigated in several configurations, where we demonstrate the complexity of the resulting nonlinear frequency curves in terms of modal interactions and bifurcation topology transfer. The complex response curves were shown to emphasize the large number of nontrivial solution branches, even for a small number of coupled oscillators. This can serve as a hint of the important number of multimodal solutions, expected for large number of oscillators. Besides, when the number of coupled oscillators increases, the collective dynamics becomes more complex with a large number of bifurcation points and multimodal interactions over a wide frequency range. Finally, the basins of attraction have been analyzed, precisely in the multistability domain which confirms the robustness of the multi-mode solutions. From a numerical analysis point of view, this problem consists a veritable challenge that we will attempt to study in a future work.

In practice, the nonlinearity can be functionalized in such periodic structures in order to generate particular collective dynamics suitable for several applications. Indeed, the model can be used as a design tool in order to increase the number of bifurcations for jump-based multiple mass sensing in micro and nanotechnology or obtaining a large number of stable branches for energy scavenging or trapping applications. Moreover, the stability of these branches can be tuned in the frequency domain for ultra wide bandwidth filters. Finally, the study of collective nonlinear dynamics of coupled mechanical resonators may serve to identify the Intrinsic Localized Modes (ILMs) [47] which can be used as waveguides in vibro-acoustics.

Acknowledgements This project has been performed in cooperation with the Labex ACTION program (contract ANR-11-LABX-01-01).

Appendix A

Substituting Equation (5) into the EOM term by term. Up to the order $\varepsilon^{\frac{3}{2}}$, we obtain:

$$\begin{aligned} (u_{n+1} - 2u_n + u_{n-1}) = & \\ & - 4\varepsilon^{\frac{1}{2}} \sum_{m=1}^N \sin^2\left(\frac{q_m}{2}\right) \sin(nq_m) (A_m e^{i\omega_m t} + c.c.) \\ & + \varepsilon^{\frac{3}{2}} (u_{n+1}^{(1)} - 2u_n^{(1)} + u_{n-1}^{(1)}), \end{aligned}$$

$$\begin{aligned} u_n^3 = \frac{\varepsilon^{\frac{3}{2}}}{4} \sum_{j,k,l} \{ & T^{(-j,k,l)} + T^{(j,-k,l)} + T^{(j,k,-l)} - T^{(j,k,l)} \} \times \\ & \{ A_j A_k A_l e^{i(\omega_j + \omega_k + \omega_l)t} + 3A_j A_k A_l^* e^{i(\omega_j + \omega_k - \omega_l)t} + c.c. \}, \end{aligned}$$

$$\begin{aligned} u_n^2 \dot{u}_n = 4\varepsilon^{\frac{3}{2}} \sum_{j,k,l} \{ & T^{(-j,k,l)} + T^{(j,-k,l)} + T^{(j,k,-l)} - T^{(j,k,l)} \} \\ & \times (A_j e^{i\omega_j t} + c.c.) (A_k e^{i\omega_k t} + c.c.) (i\omega_l A_l e^{i\omega_l t} + c.c.), \end{aligned}$$

$$\begin{aligned}
& [(u_n - u_{n+1})^3 + (u_n - u_{n-1})^3] \\
& = 4\varepsilon^{\frac{3}{2}} \sum_{j,k,l} \Pi_{j,k,l} \{S^{(-j,k,l)} + S^{(j,-k,l)} + S^{(j,k,-l)} + S^{(j,k,l)}\} \\
& \times \{A_j A_k A_l e^{i(\omega_j + \omega_k + \omega_l)t} + 3A_j A_k A_l^* e^{i(\omega_j + \omega_k - \omega_l)t} + c.c.\},
\end{aligned}$$

$$\begin{aligned}
& [(u_n - u_{n+1})^2(\dot{u}_n - \dot{u}_{n+1}) + (u_n - u_{n-1})^2(\dot{u}_n - \dot{u}_{n-1})] \\
& = \frac{\varepsilon^{\frac{3}{2}}}{4} \sum_{j,k,l} \Pi_{j,k,l} \{S^{(-j,k,l)} + S^{(j,-k,l)} + S^{(j,k,-l)} + S^{(j,k,l)}\} \\
& \times (A_j e^{i\omega_j t} + c.c.)(A_k e^{i\omega_k t} + c.c.)(i\omega_l A_l e^{i\omega_l t} + c.c.),
\end{aligned}$$

with:

$$T^{(j,k,l)} = \sin[n(\operatorname{sgn}(j)q_j + \operatorname{sgn}(k)q_k + \operatorname{sgn}(l)q_l)]$$

$$S^{(j,k,l)} = \sin\left[\frac{\operatorname{sgn}(j)q_j + \operatorname{sgn}(k)q_k + \operatorname{sgn}(l)q_l}{2}\right] T^{(j,k,l)}$$

$$\Pi_{j,k,l} = \sin\left(\frac{q_j}{2}\right) \sin\left(\frac{q_k}{2}\right) \sin\left(\frac{q_l}{2}\right)$$

Appendix B

The two delta functions, defined in terms of Kronecker deltas are:

$$\begin{aligned}
\Delta_{jkl;m}^{(1)} & = \delta_{-j+k+l,m} - \delta_{-j+k+l,m} - \delta_{-j+k+l,2(N+1)-m} \\
& + \delta_{j-k+l,m} - \delta_{j-k+l,m} - \delta_{j-k+l,2(N+1)-m} \\
& + \delta_{j+k-l,m} - \delta_{j+k-l,m} - \delta_{j+k-l,2(N+1)-m} \\
& - \delta_{j+k+l,m} + \delta_{j+k+l,2(N+1)-m} - \delta_{j+k+l,2(N+1)+m}
\end{aligned}$$

and

$$\begin{aligned}
\Delta_{jkl;m}^{(2)} & = \delta_{-j+k+l,m} + \delta_{-j+k+l,m} + \delta_{-j+k+l,2(N+1)-m} \\
& + \delta_{j-k+l,m} + \delta_{j-k+l,m} - \delta_{j-k+l,2(N+1)-m} \\
& + \delta_{j+k-l,m} + \delta_{j+k-l,m} - \delta_{j+k-l,2(N+1)-m} \\
& + \delta_{j+k+l,m} - \delta_{j+k+l,2(N+1)-m} - \delta_{j+k+l,2(N+1)+m}
\end{aligned}$$

References

1. L. Brillouin. *Wave Propagation in Periodic Structures: Electric Filters and Crystal Lattices*. Dover Publications, Dover Publications, 1953.
2. D.J. Mead. A general theory of harmonic wave propagation in linear periodic systems with multiple coupling. *Journal of Sound and Vibration*, 27(2):235 – 260, 1973.
3. R.S. Langley. The response of two-dimensional periodic structures to point harmonic forcing. *Journal of Sound and Vibration*, 197(4):447 – 469, 1996.
4. R.S. Langley, N.S. Bardell, and H.M. Ruivo. The response of two-dimensional periodic structures to harmonic point loading: a theoretical and experimental study of beam grillage. *Journal of Sound and Vibration*, 207(4):521 – 535, 1997.

5. J.S. Jensen. Phononic band gaps and vibrations in one- and two-dimensional massspring structures. *Journal of Sound and Vibration*, 266(5):1053 – 1078, 2003.
6. M. Collet, K.A. Cunefare, and M.N. Ichchou. Wave motion optimization in periodically distributed shunted piezocomposite beam structures. *Journal of Intelligent Material Systems and Structures*, 20(7):787–808, 2009.
7. M. Collet, M. Ouisse, M. Ruzzene, and M.N. Ichchou. Floquetbloch decomposition for the computation of dispersion of two-dimensional periodic, damped mechanical systems. *International Journal of Solids and Structures*, 48(20):2837 – 2848, 2011.
8. Y. V. Kartashov, B. A. Malomed, and L. Torner. Solitons in nonlinear lattices. *Rev. Mod. Phys.*, 83:247–305, Apr 2011.
9. Nikolaos K. Efremidis J. W. Fleischer, Mordechai Segev and Demetrios N. Christodoulides. Observation of two-dimensional discrete solitons in optically induced nonlinear photonic lattices. *Nature*, 422:147–150, 2003.
10. Tristram J. Alexander, Andrey A. Sukhorukov, and Yuri S. Kivshar. Asymmetric vortex solitons in nonlinear periodic lattices. *Phys. Rev. Lett.*, 93:063901, Aug 2004.
11. Xu Quan and Tian Qiang. Periodic, quasiperiodic and chaotic discrete breathers in a parametrical driven two-dimensional discrete klein-gordon lattice. *Chinese Physics Letters*, 26(4):040501, 2009.
12. S. Flach and A. Gorbach. Discrete breathers in fermipastulam lattices. *Chaos: An Interdisciplinary Journal of Nonlinear Science*, 15(1):–, 2005.
13. G. Chakraborty and A.K. Mallik. Dynamics of a weakly non-linear periodic chain. *International Journal of Non-Linear Mechanics*, 36(2):375 – 389, 2001.
14. F. Romeo and G. Rega. Wave propagation properties in oscillatory chains with cubic nonlinearities via nonlinear map approach. *Chaos, Solitons & Fractals*, 27(3):606 – 617, 2006.
15. F. Romeo and G. Rega. Periodic and localized solutions in chains of oscillators with softening or hardening cubic nonlinearity. *Meccanica*, 50(3):721–730, 2015.
16. K. Manktelow, R. K. Narisetti, M. J. Leamy, and M. Ruzzene. Finite-element based perturbation analysis of wave propagation in nonlinear periodic structures. *Mechanical Systems and Signal Processing*, 39(12):32 – 46, 2013.
17. K. Manktelow, M. J. Leamy, and M. Ruzzene. Multiple scales analysis of wavewave interactions in a cubically nonlinear monoatomic chain. *Nonlinear Dynamics*, 63(1-2):193–203, 2011.
18. A. Marathe and A. Chatterjee. Wave attenuation in nonlinear periodic structures using harmonic balance and multiple scales. *Journal of Sound and Vibration*, 289(45):871 – 888, 2006.
19. B.S. Lazarov and J.S. Jensen. Low-frequency band gaps in chains with attached non-linear oscillators. *International Journal of Non-Linear Mechanics*, 42(10):1186 – 1193, 2007.
20. N. Boechler, C. Daraio, R. K. Narisetti, M. Ruzzene, and M.J. Leamy. Analytical and experimental analysis of bandgaps in nonlinear one dimensional periodic structures. In Tsung-Tsong Wu and Chien-Ching Ma, editors, *IUTAM Symposium on Recent Advances of Acoustic Waves in Solids*, volume 26 of *IUTAM Bookseries*, pages 209–219. Springer Netherlands, 2010.
21. G. Theocharis, N. Boechler, and C. Daraio. Nonlinear periodic phononic structures and granular crystals. In Pierre A. Deymier, editor, *Acoustic Metamaterials and Phononic Crystals*, volume 173 of *Springer Series in Solid-State Sciences*, pages 217–251. Springer Berlin Heidelberg, 2013.
22. Georg Heinrich, Max Ludwig, Jiang Qian, Björn Kubala, and Florian Marquardt. Collective dynamics in optomechanical arrays. *Phys. Rev. Lett.*, 107:043603, Jul 2011.
23. R.E. Slusher and B.J. Eggleton. *Nonlinear Photonic Crystals*. Physics and Astronomy Online Library. Springer, 2003.
24. S. Gutschmidt and O. Gottlieb. Nonlinear dynamic behavior of a microbeam array subject to parametric actuation at low, medium and large dc-voltages. *Nonlinear Dynamics*, 67(1):1–36, 2012.
25. R. Lifshitz and M. C. Cross. *Nonlinear Dynamics of Nanomechanical and Micromechanical Resonators*. Wiley, 2008.
26. A.H. Nayfeh and L.D. Zavodney. The response of two-degree-of-freedom systems with quadratic nonlinearities to a combination parametric resonance. *Journal of Sound and Vibration*, 107(2):329 – 350, 1986.
27. A.H. Nayfeh. The response of multidegree-of-freedom systems with quadratic non-linearities to a harmonic parametric resonance. *Journal of Sound and Vibration*, 90(2):237 – 244, 1983.
28. R. Lifshitz and M. C. Cross. Response of parametrically driven nonlinear coupled oscillators with application to micromechanical and nanomechanical resonator arrays. *Physical review B*, 67, 2003.
29. E. Perkins and B. Balachandran. Noise-enhanced response of nonlinear oscillators. *Procedia {IUTAM}*, 5(0):59 – 68, 2012. {IUTAM} Symposium on 50 Years of Chaos: Applied and Theoretical.
30. N. Kacem, S. Baguet, R. Dufour, and S. Hentz. Stability control of nonlinear micromechanical resonators under simultaneous primary and superharmonic resonances. *Applied Physics Letters*, 98(19):–, 2011.

31. Hai Nguyen. Simultaneous resonances involving two mode shapes of parametrically-excited rectangular plates. *Journal of Sound and Vibration*, 332(20):5103 – 5114, 2013.
32. R.H. Plaut, N. HaQuang, and D.T. Mook. Simultaneous resonances in non-linear structural vibrations under two-frequency excitation. *Journal of Sound and Vibration*, 106(3):361 – 376, 1986.
33. B Cochelin. A path-following technique via an asymptotic-numerical method. *Computers and Structures*, 53:1181–1192, 1994.
34. Eyal Buks and Michael L. Roukes. Electrically tunable collective response in a coupled micromechanical array. *Microelectromechanical Systems, Journal of*, 11(6):802–807, Dec 2002.
35. Manlab 2.0, an interactive continuation software. (last viewed 3/16/2011) Software written by S. Karkar, R. Arquier, B. Cochelin, C. Vergez, O. Thomas and A. Lazarus.
36. P. Vannucci, B. Cochelin, N. Damil, and M. Potier-Ferry. An asymptotic-numerical method to compute bifurcating branches. *International Journal for Numerical Methods in Engineering*, 41(8):1365–1389, 1998.
37. I. Abed, N. Kacem, M.L. Bouazizi, and N. Bouhaddi. Nonlinear 2-dofs vibration energy harvester based on magnetic levitation. In Alfred Wicks, editor, *Shock and Vibration, Aircraft/Aerospace, and Energy Harvesting, Volume 9*, Conference Proceedings of the Society for Experimental Mechanics Series, pages 39–45. Springer International Publishing, 2015.
38. N Kacem, J Arcamone, F Perez-Murano, and S Hentz. Dynamic range enhancement of nonlinear nanomechanical resonant cantilevers for high sensitive nems gas/mass sensors applications. *Journal of Micromechanics and Microengineering*, 20(4):045023, 2010.
39. H. W. C. Kozinsky, I. Postma, A. Kogan, O. Husain, and M. L. Roukes. Basins of attraction of a nonlinear nanomechanical resonator. *Physical Review Letters*, 99(20), 2007.
40. I. Iiwa and K. Grygiel. Periodic orbits, basins of attraction and chaotic beats in two coupled kerr oscillators. *Nonlinear Dynamics*, 67(1):755–765, 2012.
41. Laura Ruzziconi, MohammadI. Younis, and Stefano Lenci. Multistability in an electrically actuated carbon nanotube: a dynamical integrity perspective. *Nonlinear Dynamics*, 74(3):533–549, 2013.
42. V.-N. Nguyen, S. Baguet, C.-H. Lamarque, and R. Dufour. Bifurcation-based micro/nanoelectromechanical mass detection. *Nonlinear Dynamics*, 79(1):647–662, 2015.
43. M.S. Soliman and J.M.T. Thompson. Integrity measures quantifying the erosion of smooth and fractal basins of attraction. *Journal of Sound and Vibration*, 135(3):453 – 475, 1989.
44. S. Lenci and G. Rega. Competing dynamic solutions in a parametrically excited pendulum: Attractor robustness and basin integrity. *Journal of Computational and Nonlinear Dynamics*, 3(1555-1415), 2008.
45. G. Rega and S. Lenci. Identifying, evaluating, and controlling dynamical integrity measures in non-linear mechanical oscillators. *Nonlinear Analysis: Theory, Methods & Applications*, 63(57):902 – 914, 2005. Invited Talks from the Fourth World Congress of Nonlinear Analysts (WCNA 2004) Invited Talks from the Fourth World Congress of Nonlinear Analysts (WCNA 2004).
46. Giuseppe Rega and Stefano Lenci. Dynamical integrity and control of nonlinear mechanical oscillators. *Journal of Vibration and Control*, 14(1-2):159–179, 2008.
47. Eyal Kenig, Boris A. Malomed, M. C. Cross, and R. Lifshitz. Intrinsic localized modes in parametrically driven arrays of nonlinear resonators. *Phys. Rev. E*, 80:046202, Oct 2009.